

Orbital ordering in FeV₂O₄: Spinel with two orbitally active sites

Soumyajit Sarkar and T. Saha-Dasgupta

Department of Materials Science, S.N. Bose National Centre for Basic Sciences, Kolkata, India

(Received 14 September 2011; revised manuscript received 22 October 2011; published 5 December 2011)

By employing first-principles electronic structure calculations, we investigate orbital ordering in FeV₂O₄, a spinel with orbital degrees of freedom both at Fe and V sites that exhibits two tetragonal phases, one compressed at high temperature and another elongated at low temperature. Our first-principles study shows the ferro-orbital ordering of $d_{x^2-y^2}$ and $d_{3z^2-r^2}$ types at Fe sites at the high- and low-temperature phases, respectively. The orbital ordering at V sites is found to consist of orbital chains running along different directions with orbitals rotated alternatively within each chain, similar to that found for MnV₂O₄ [S. Sarkar *et al.*, *Phys. Rev. Lett.* **102**, 216405 (2009)]. Further, we find that the single-ion anisotropy effect with hard and easy c axis favors the compressed and elongated tetrahedral shapes. This gives rise to magnetocrystalline anisotropy-dependent shapes, similar to that reported in the context of rare-earth-based magnetic shape memory alloys.

DOI: 10.1103/PhysRevB.84.235112

PACS number(s): 71.20.-b, 71.15.Mb, 71.70.Ej

I. INTRODUCTION

Transition-metal-oxide (TMO) spinels have attracted considerable attention in recent times due to intricate interplay among charge, spin, and orbital degree of freedom, giving rise to fascinating properties. A lot of work has been carried out for normal spinels of general formula AB_2O_4 , which consist of AO_4 tetrahedral units connected to BO_6 octahedral units. These compounds are often reported¹ to undergo transitions from cubic to tetragonal symmetries, accompanied by orbital ordering as well as magnetic ordering at low temperature. So far, theoretical investigations have been mostly restricted to spinels having either an orbitally active B site like V^{3+} as in MnV₂O₄,² CdV₂O₄, or ZnV₂O₄³ or an orbitally active A site like Fe^{2+} as in FeCr₂O₄.⁴ For the former, the d^2 configuration of V in threefold degenerate manifold of octahedrally split t_{2g} 's gives rise to orbital degeneracy, while for the latter, the d^6 configuration of Fe, with a local $S = 2$ moment and one hole in twofold degenerate manifold of tetrahedrally split e states, gives rise to orbital degeneracy. What happens if both A and B sites become orbitally active? Such a situation arises in the case of FeV₂O₄. This compound is reported⁵ to exhibit two tetragonal phases, one at relatively higher temperature (140–110 K) and another at relatively lower temperature (<70 K). The symmetry above 140 K is cubic. It is curious that while for the high-temperature tetragonal (HT-T) phase the c axis is shorter than the other axis ($a = b$), for the low-temperature tetragonal (LT-T) phase it is opposite, with the c axis being longer than the other axis.⁶ The opposite nature of the c/a ratio in the HT-T and LT-T phases is accommodated by the presence of an orthorhombic phase in the intervening temperature range of 110–70 K. As shown in Fig. 1, the VO₆ octahedra are compressed in both HT-T and LT-T phases, with the degree of compression being larger in the LT-T phase. FeO₄ tetrahedra, on the other hand, are compressed in the HT-T phase and elongated in the LT-T phase.⁶ The presence of two tetragonal phases of two different shapes is in contrast to the situations of only A site or only B site orbitally active spinels, for which the tetragonal phase is either compressed as in MnV₂O₄² and ZnV₂O₄³ or elongated as in Mn₃O₄ and CoMn₂O₄.⁷

II. METHODOLOGY

In this paper, we carried out a detailed density functional theory (DFT)-based investigation of the electronic structure of HT-T and LT-T phases, studied their commonalities and differences, and investigated the origin of the existence of two different tetragonal phases. Calculations were carried out in the linear augmented plane wave (LAPW) as implemented in the WIEN2K code,⁸ as well as the muffin-tin orbital (MTO)-based N th order MTO (NMTO) method as implemented in the STUTTGART code.⁹ The NMTO-downfolding calculation was used to determine the crystal field splitting at Fe and V sites. For this purpose, NMTO-downfolding calculations were carried out keeping only the Fe- d and V- d states active and downfolding all the other states, including O- p states. The on-site block of the real-space Hamiltonian in the Fe- d and V- d bases gives the crystal field splitting. The density of states and electron-density plots as well as structural optimizations were obtained with LAPW calculations with no shape approximation for the potential. For the LAPW calculations, the number of plane waves was restricted using the criteria of muffin-tin radius multiplied by k_{\max} , yielding a value of 7. The Brillouin zone (BZ) was sampled with 196 irreducible k points for self-consistent calculations. The exchange-correlation functional was chosen to be that of generalized gradient approximation (GGA).¹⁰ Strong electron-electron correlation effects are expected to be present in the unfilled d shell of TM sites of a TMO spinel, which are insufficiently captured by GGA. Methods like self-interaction-corrected local spin density¹¹ or hybrid functionals¹² have been used to include correlation effects in spinels. In the present study, the missing Coulomb interaction beyond GGA was supplemented through additional on-site Coulomb interaction, expressed in terms of Coulomb U and the Hund's rule coupling, J_H through GGA + U calculations.¹³ For calculations including spin-orbit (SO) coupling, it was included in scalar relativistic form as a perturbation to the original Hamiltonian. The NMTO calculations relies on the linear muffin-tin orbital (LMTO)¹⁴ for the self-consistent potentials. The self-consistent LMTO calculations have been carried out with choices of two empty spheres to space fill. The muffin-tin radii at Fe, V, and O sites

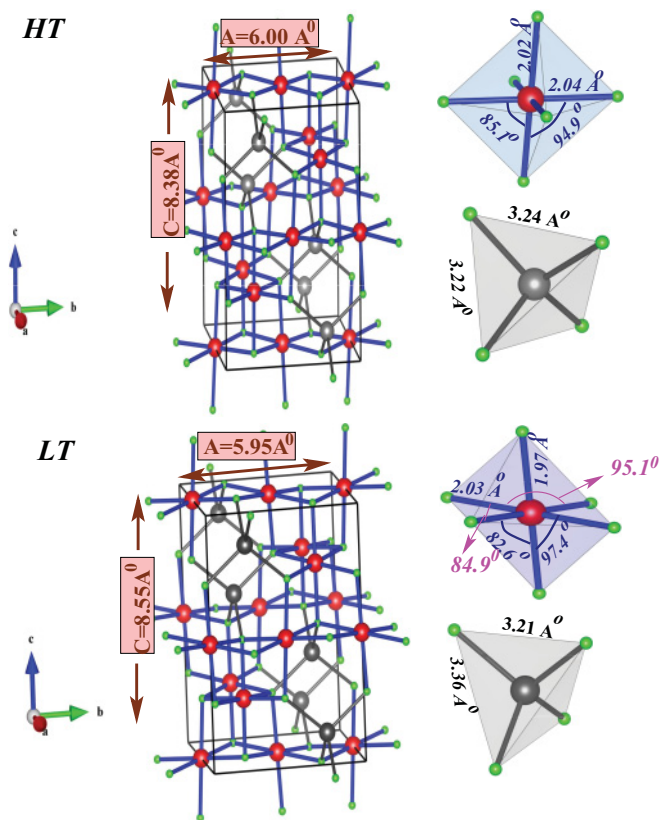


FIG. 1. (Color online) The crystal structures of HT-T and LT-T phases of FeV_2O_4 . O sites are indicated with small balls, while Fe and V sites are indicated with grey (light grey) and red (dark grey) medium-sized balls. The cubic (a , c) and tetragonal (A , C) setting of lattice parameters are related by $a = A\sqrt{2}$ and $c = C$, giving rise to $c/a = 0.988$ and 1.016 for HT-T and LT-T structures, respectively. The VO_6 and FeO_4 structural units for both structures are shown separately, along with the various bond lengths and bond angles.

were chosen to be 1.38 \AA , 1.43 \AA , and 0.95 \AA , respectively. The consistency of LAPW and LMTO calculations have been cross-checked in terms of density of states and band structure plots.

III. RESULTS AND DISCUSSIONS

A. Calculations within GGA

Figures 2 and 3 show the spin-polarized density of states (DOS) calculated within GGA corresponding to HT-T and LT-T phases, projected on to Fe- d and V- d characters respectively. According to magnetic measurements, the magnetic ordering with antiparallel alignment of Fe and V ions takes place at $T_c \approx 110 \text{ K}$. The HT-T phase is, therefore, in paramagnetic (PM) state, which for correlated TMO spinels consists of local moments at TM sites, oriented randomly. Within periodic DFT calculations, as in the present study, it is not possible to simulate the PM state with randomly oriented local moments. Hence, we have carried out spin-polarized calculations for both HT-T and LT-T phases, which is expected to provide knowledge of correct spin states of Fe and V and correct occupations of various d levels in the presence of local moments. The spin-polarized calculation

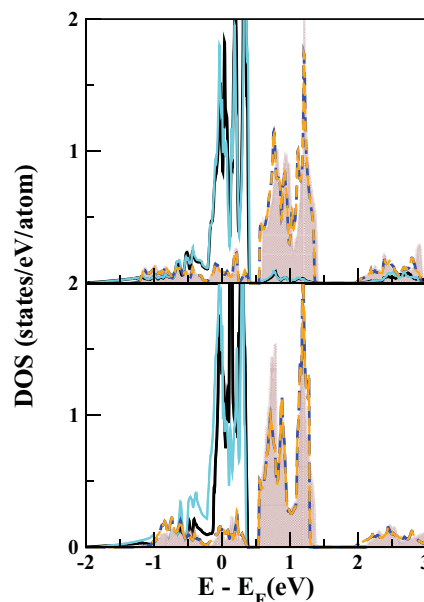


FIG. 2. (Color online) Spin-polarized GGA DOS projected onto Fe- d states, calculated in the LAPW basis. The top and bottom panels correspond to plots for HT-T and LT-T respectively. The DOSs shown are for the minority spin channel of Fe. Contributions of $d_{3z^2-r^2}$, $d_{x^2-y^2}$, d_{xz} , d_{yz} , and d_{xy} are represented by solid black, solid cyan (light grey), dashed blue (dark grey), dashed orange (light grey), and shaded regions respectively.

gives rise to ferrimagnetic alignments of Fe and V moments, in accordance with experimental observation⁵ of ferrimagnetism at low temperature. The DOSs are shown for the majority (minority) channel of V (Fe), as the states in the other spin channel are either completely empty or completely occupied.

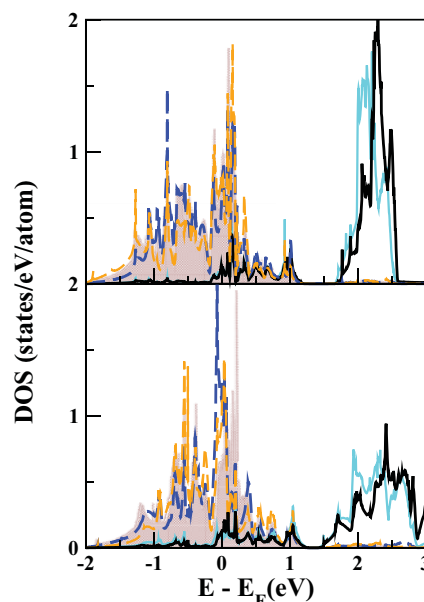


FIG. 3. (Color online) Spin-polarized GGA DOS projected onto V- d states, calculated in the LAPW basis. The top and bottom panels correspond to plots for HT-T and LT-T respectively. The DOSs shown are for the majority spin channel of V. The conventions of different line styles are the same as in Fig. 2.

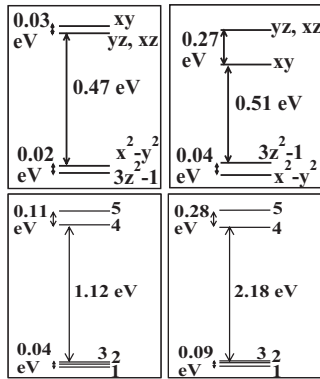


FIG. 4. The crystal field splittings of Fe- d (top panels) and V- d (bottom panels) states, computed by the NMTO-downfolding technique. The left and right panels correspond to plots for HT-T and LT-T respectively. For V, due to mixed d characters, the positions of levels $|1\rangle \dots |5\rangle$ are shown.

Focusing on the Fe- d -derived states, we find clear grouping of states, one around Fermi energy (E_F) and another above E_F , at ~ 1 eV, the first and second grouping being of e and t_2 characters respectively. The tetragonal distortion of FeO₄ tetrahedra, as shown in Fig. 1, measured in terms of O-O bond lengths (d_{O-O}) along $\langle 110 \rangle$ and $\langle 001 \rangle$ directions, $\frac{d_{O-O}(\langle 101 \rangle)}{d_{O-O}(\langle 110 \rangle)}$, is ~ 0.99 for the HT-T phase and ~ 1.05 for the LT-T phase. This distortion lifts the degeneracy between two e states, with $d_{3z^2-r^2}$ being below (above) $d_{x^2-y^2}$ for HT-T (LT-T). The crystal field splitting of Fe- d is shown in top panels of Fig. 4. The tetragonal distortion also leads to splitting within t_2 states, with doubly degenerate $d_{yz,xz}$ states and singly degenerate d_{xy} , the relative positioning of the states

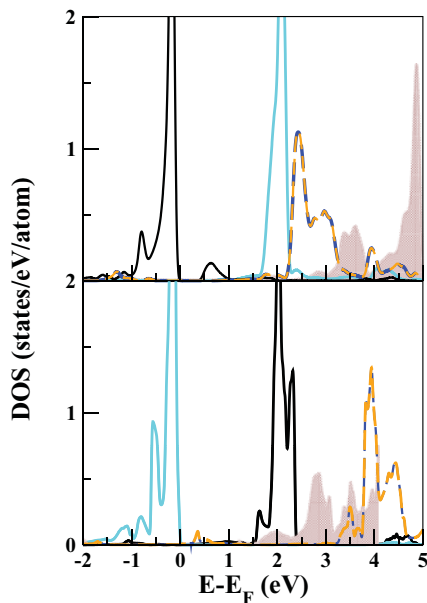


FIG. 5. (Color online) GGA + U DOS projected onto Fe- d states for HT-T (top panel) and LT-T (bottom panel), calculated in the LAPW basis. The conventions of different line styles are the same as in Fig. 2. The bottom panels show the plot of charge density, demonstrating the orbital ordering at Fe site.

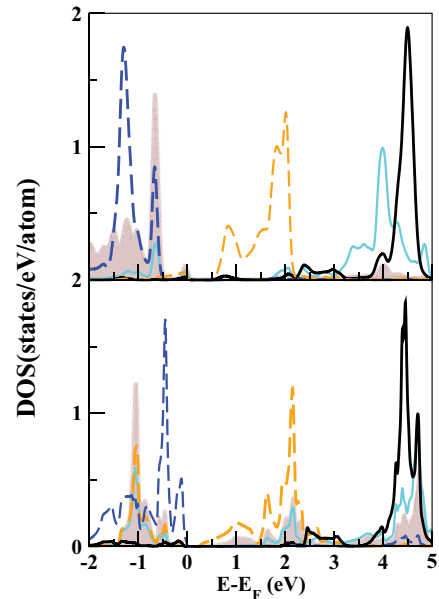


FIG. 6. (Color online) GGA + U DOS projected onto V- d states for HT-T (top panel) and LT-T (bottom panel), calculated in the LAPW basis. The conventions of different line styles are same as in Fig. 2.

being given by the nature of distortion as shown in the insets.

Focusing on V- d -derived states, the groupings in t_{2g} and e_g states are evident with t_{2g} states being lower in energy compared to e_g , as expected for octahedral crystal field. The VO₆ octahedra, in addition to tetragonal distortion with V-O bond length along the $\langle 001 \rangle$ direction being smaller than that along the $\langle 100 \rangle$ direction, also shows trigonal distortion, which makes the O-V-O angle deviate from 90° . The trigonal distortion coupled with tetragonal distortion not only lifts the degeneracy of V- d states completely but also mixes them. The lowest three levels (referred to as $|1\rangle$, $|2\rangle$, $|3\rangle$) are given by predominant contributions of d_{xy} , d_{yz} , and d_{xz} characters, as listed below for HT-T and LT-T:

$$\begin{aligned}
 |1\rangle^{\text{HT}} &= -0.239|d_{xz}\rangle + 0.969|d_{xy}\rangle + 0.050|d_{3z^2-r^2}\rangle, \\
 |2\rangle^{\text{HT}} &= -0.060|d_{x^2-y^2}\rangle - 0.998|d_{yz}\rangle, \\
 |3\rangle^{\text{HT}} &= 0.970|d_{xz}\rangle + 0.240|d_{xy}\rangle - 0.020|d_{3z^2-r^2}\rangle, \\
 |1\rangle^{\text{LT}} &= -0.239|d_{yz}\rangle + 0.970|d_{xy}\rangle, \\
 |2\rangle^{\text{LT}} &= 0.119|d_{x^2-y^2}\rangle + 0.990|d_{xz}\rangle, \\
 |3\rangle^{\text{LT}} &= 0.970|d_{yz}\rangle - 0.238|d_{xy}\rangle + 0.025|d_{3z^2-r^2}\rangle.
 \end{aligned}$$

The details of the crystal field splitting at the V site are shown in the bottom panels of Fig. 4.

B. Calculation within GGA + U

Figures 5 and 6 show the GGA + U DOSs for Fe- d and V- d projected states, respectively. In GGA + U calculations, U and J_H are free parameters which need to be chosen. We have carried out calculations considering several choices of U values. The DOSs shown in Figs. 5 and 6 are obtained

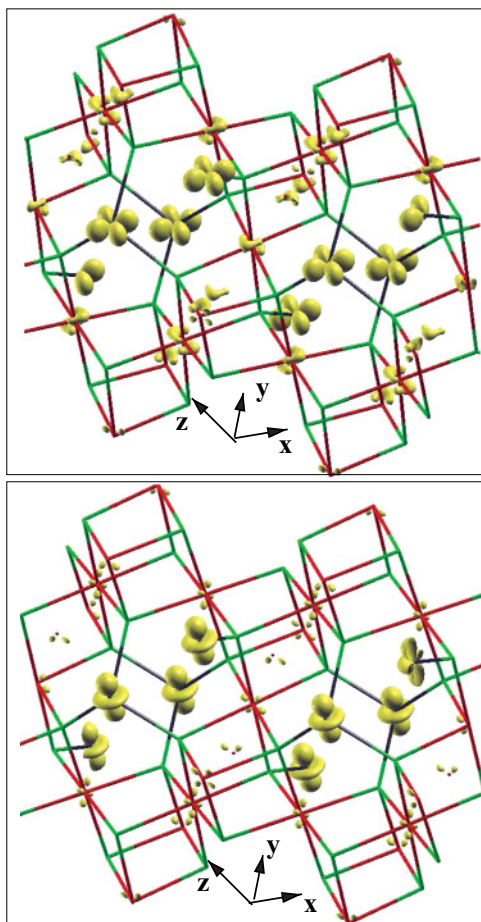


FIG. 7. (Color online) The plot of charge density calculated within GGA + U , demonstrating the orbital ordering at the Fe site for HT-T (top panel) and LT-T (bottom panel).

with U values of 4.5 eV at Fe and V sites. J_H is chosen to be 1 eV. Variations of U values do not change the essential results related to orbital ordering, though they do affect the details, for example, the size of the gap. The above choice of U values leads to an insulating solution for both HT-T and LT-T. As shown in Fig. 5, the effect of U , which makes the more occupied states completely occupied and less occupied states empty, drives the minority spin Fe $d_{3z^2-r^2}$ ($d_{x^2-y^2}$) states completely occupied and Fe $d_{x^2-y^2}$ ($d_{3z^2-r^2}$) states completely empty for HT-T (LT-T). This leads to a ferro-orbital ordering of $d_{x^2-y^2}$ type with the hole residing in the $d_{x^2-y^2}$ orbital in the HT-T case and of $d_{3z^2-r^2}$ with the hole residing in the $d_{3z^2-r^2}$ orbital in the LT-T case, as shown in Fig. 7.

The low-energy states of V- d GGA + U DOS (*cf.* Fig. 6) show the major peaks corresponding to the mixed t_{2g} states, $|1\rangle, |2\rangle$, and $|3\rangle$, which get filled by two d electrons of V. The corresponding orbital ordering at the V site, shown in Fig. 8, looks very similar to that found on MnV_2O_4 ,² in the sense it represents a ferro-orbital ordering with formation of orbital chains in which the orbital rotates from one site to another both between and within the chain due to the presence of a co-operative type of local trigonal distortion at the V site.

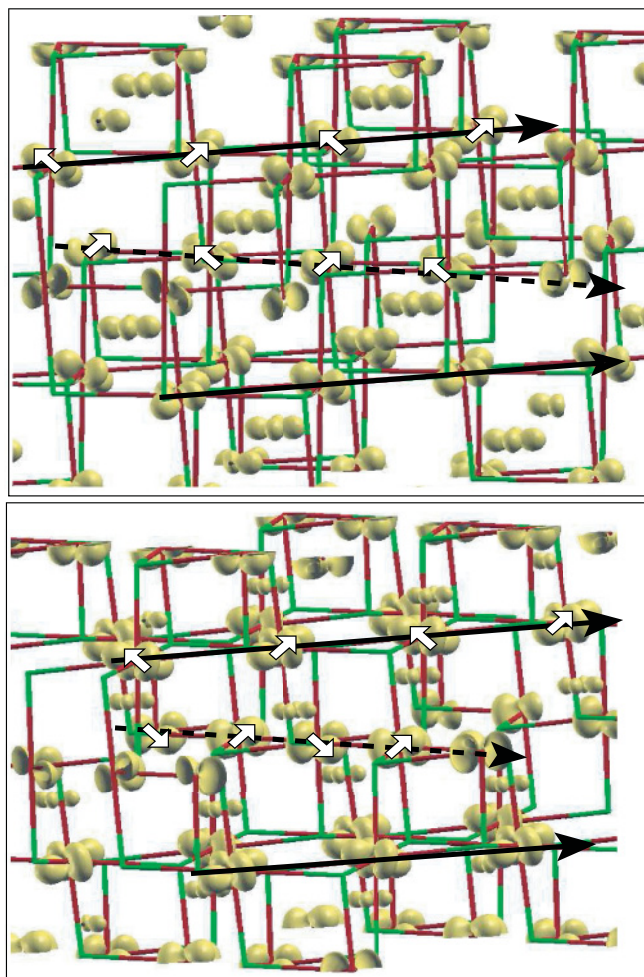


FIG. 8. (Color online) The plot of charge density calculated within GGA + U , demonstrating the orbital ordering at the V site for HT-T (top panel) and LT-T (bottom panel). The arrows mark the rotation of the orbitals as one moves to neighboring V sites within a given orbital chain, while the solid and dashed lines mark the orbital chains.

C. Effect of spin-orbit interaction

The SO effect has been often considered to play an important role in orbital ordering in spinels.¹⁵ The orbital moment is found to be significant for V-based spinels like ZnV_2O_4 ³ and MnV_2O_4 ² with two electrons in the t_{2g} manifold, as SO interaction within the t_{2g} manifold produces orbital polarization for t_{2g}^n configurations with $n = 1, 2, 4, 5$.¹⁶ The counterintuitive and rather large orbital moment has been reported for e levels of Fe in FeCr_2S_4 ,¹⁷ which has been argued to happen through coupling with empty Fe t_2 orbitals. Therefore, in order to probe the effect of SO, we carried out GGA + U + SO calculations. The orbital moments at the Fe site are found to be $\sim 0.11\text{--}0.12 \mu_B$ pointed in the same direction as the spin moment of magnitude $\sim 3.4\text{--}3.5 \mu_B$, while that at V site is found to be $\sim 0.09\text{--}0.1 \mu_B$ directed in the opposite direction of the spin moment of magnitude $\sim 1.6\text{--}1.7 \mu_B$, in agreement with more than half-filled and less than half-filled d occupancies of Fe and V, respectively.¹⁸ Following the observation of significant orbital moments at both Fe and V sites, in the next step we investigate the possible

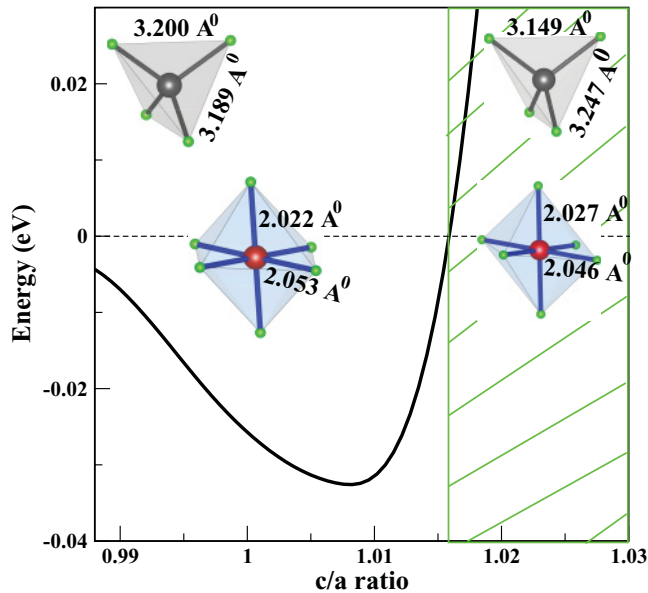


FIG. 9. (Color online) The difference of GGA + U + SO energies, calculated in the LAPW basis, with spin quantization axis pointed along [110] and [001], plotted for various c/a ratios. The VO_6 and FeO_4 units of the optimized structures for $c/a = 0.99$ and $c/a = 1.02$ are shown in the unhatched and hatched regions, respectively.

role of SO in the structural aspects. For this purpose, we carried out GGA + U + SO calculations considering tetragonal structures of varied c/a ratios, from values < 1 to values > 1 . For each c/a ratio, all the atomic positions as well as volume are optimized. Two sets of calculations are carried out, one with the spin quantization axis pointed along the [001] direction and another with the spin quantization axis pointed along the [110] direction.¹⁹ The results are summarized in Fig. 9. Interestingly, we find that while $c/a < 1$ is favored with the spin quantization axis pointed along the [110] direction, beyond a critical value of c/a , which turns out to be 1.016, $c/a > 1$ is favored with the spin quantization axis pointed along the [001] direction. It is interesting to note that the $c/a > 1$ structure does contain elongated FeO_4 tetrahedral units and compressed VO_6 octahedral units, as shown in the inset of Fig. 9, similar to experimental observation. This leads to a situation where the single-ion anisotropy influences the shape of the solid. A similar effect has been observed recently in rare-earth-based magnetic shape memory (MSM) materials like RCu_2 ($R = \text{rare}$

earth).²⁰ The single-ion anisotropy-driven effect is operative even in the paramagnetic phase, as discussed for RCu_2 , and therefore expected for the HT-T phase of FeV_2O_4 . For the FeCr_2S_4 spinel, the single-ion anisotropy at the Fe site was found to be in plane¹⁷ while that of the V site in ZnV_2O_4 ³ or MnV_2O_4 ² is found to be out of plane.²¹ The interplay of the single-ion anisotropies of Fe and V, which gets influenced by the magnetic exchange between Fe and V below T_c , leads to change in the overall spin quantization axis from in plane to out of plane in moving from HT to LT and subsequent change in the shape. The change of structure therefore is caused by the change in the direction of magnetic anisotropy from in plane to out of plane, helped by the setting up of magnetic exchange between Fe and V, introducing a somewhat different mechanism of magnetostriction than in commonly known examples. The single-ion anisotropy-driven rare-earth MSM materials have been reported²⁰ to exhibit giant magnetostrain of the order of 1%. Interestingly enough, a similar effect has been also reported for FeV_2O_4 .⁶

IV. CONCLUSION

In conclusion, using DFT calculations we have investigated the orbital ordering in FeV_2O_4 , which contains both orbitally active A and B sites. In contrast to spinels with single orbitally active sites, which show only one kind of tetragonal phase, this compound is reported⁵ to show two tetragonal phases, one compressed at high temperature and another elongated at low temperature. We find that the orbital ordering at the Fe site is a ferro-orbital ordering of the $d_{x^2-y^2}$ kind at high temperature and of the $d_{3z^2-r^2}$ kind at low temperature, while that at the V site forms orbitally ordered chains driven by staggered trigonal distortion. We further find that the spin quantization axis pointed along the [110] direction is favored for compressed tetragonal shapes, while beyond a critical value of c/a with elongated tetragonal shape the spin quantization axis pointed along the [001] direction is favored. The switching of overall magnetocrystalline anisotropy from out of plane to in plane below T_c therefore causes a change in the shape of the tetragonal unit cell.

ACKNOWLEDGMENTS

S.S. thanks CSIR for financial support. T.S.D. acknowledges funding from DST and Advanced Materials Research Unit.

¹P. G. Radaelli, *New J. Phys.* **7**, 53 (2005).

²S. Sarkar, T. Maitra, Roser Valentí, and T. Saha-Dasgupta, *Phys. Rev. Lett.* **102**, 216405 (2009).

³T. Maitra and R. Valentí, *Phys. Rev. Lett.* **99**, 126401 (2007).

⁴A. Wold, R. J. Arnott, E. Whipple, and J. B. Goodenough, *J. Appl. Phys.* **34**, 1085 (1963).

⁵M. Tanaka, T. Tokoro, and Y. Aiyama, *J. Phys. Soc. Jpn.* **21**, 262 (1966).

⁶T. Katsufuji, T. Suzuki, H. Takei, M. Shingu, K. Kato, K. Osaka, M. Takata, H. Sagayama, and T. Arima, *J. Phys. Soc. Jpn.* **77**, 053708 (2008).

⁷R. Tackett, G. Lawes, B. C. Melot, M. Grossman, E. S. Toberer, and R. Seshadri, *Phys. Rev. B* **76**, 024409 (2007); P. J. Wojtowicz, *Phys. Rev.* **116**, 32 (1959).

⁸P. Blaha, K. Schwartz, G. K. H. Madsen, D. Kvasnicka, and J. Luitz, WIEN2K, Austria, 2001.

⁹O. K. Andersen and T. Saha-Dasgupta, *Phys. Rev. B* **62**, R16219 (2000).

¹⁰J. P. Perdew, K. Burke, and M. Ernzerhof, *Phys. Rev. Lett.* **77**, 3865 (1996).

¹¹Z. Szotek, W. M. Temmerman, D. Ködderitzsch, A. Svane, L. Petit, and H. Winter, *Phys. Rev. B* **74**, 174431 (2006).

- ¹²G. Giovannetti, A. Stroppa, S. Picozzi, D. Baldomir, V. Pardo, S. Blanco-Canosa, F. Rivadulla, S. Jodlauk, D. Niermann, J. Rohrkamp, T. Lorenz, S. Streltsov, D. I. Khomskii, and J. Hemberger, *Phys. Rev. B* **83**, 060402(R) (2011).
- ¹³V. I. Anisimov, I. V. Solovyev, M. A. Korotin, M. T. Czyżyk, and G. A. Sawatzky, *Phys. Rev. B* **48**, 16929 (1993).
- ¹⁴O. K. Andersen and O. Jepsen, *Phys. Rev. Lett.* **53**, 2571 (1984).
- ¹⁵O. Tchernyshyov, *Phys. Rev. Lett.* **93**, 157206 (2004).
- ¹⁶C. Jia, S. Onoda, N. Nagaosa, and J. H. Han, *Phys. Rev. B* **76**, 144424 (2007).
- ¹⁷S. Sarkar, M. De Raychaudhury, I. Dasgupta, and T. Saha-Dasgupta, *Phys. Rev. B* **80**, 201101(R) (2009).
- ¹⁸There is small variation in magnitudes of moments at Fe and V sites between the HT-T and LT-T structures.
- ¹⁹Calculated total energies at $T = 0$ K showed the $c/a > 1$ structure to be more stable with spin quantization axis pointed along the [001] direction compared to the $c/a < 1$ structure with spin quantization axis pointed along the [110] direction by about 10 meV/f.u.
- ²⁰S. Raasch, M. Doerr, A. Kreyssig, M. Loewenhaupt, M. Rotter, and J. U. Hoffmann, *Phys. Rev. B* **73**, 064402 (2006).
- ²¹M. Reehuis, A. Krimmel, N. Büttgen, A. Loidl, and A. Prokofiev, *Eur. Phys. J. B* **35**, 311 (2003); Y. Ueda, N. Fujiwara, and H. Yasuoka, *J. Phys. Soc. Jpn.* **66**, 778 (1997).